©Copyright 2014
Xiaojuan Liu

The Influence of Orbital Forcing of Tropical Insolation on the Climate and Isotopic Composition of Precipitation in South America

Xiaojuan Liu

A thesis submitted in partial fulfillment of
the requirements for the degree of

Master of Science

University of Washington

2014

Reading Committee:

David S. Battisti, Chair

Christopher S. Bretherton

Dargan M.W. Frierson

Program Authorized to Offer Degree:
Atmospheric Sciences

University of Washington

Abstract

The Influence of Orbital Forcing of Tropical Insolation on the Climate and Isotopic Composition of Precipitation in South America

Xiaojuan Liu

Chair of the Supervisory Committee:
Professor David S. Battisti
Atmospheric Sciences

The $\delta^{18}O$ of calcite ($\delta^{18}O_c$) in speleothems from South America is well correlated with austral summer (DJF) insolation, indicating the role of orbitally paced changes in insolation in changing the climate of South America. Using an isotope-enabled atmospheric general circulation model (ECHAM4.6) coupled to a slab ocean model, we study how insolation changes climate and the isotopic composition of precipitation ($\delta^{18}O_p$) of South America. Compared with times of high summertime insolation, times of low insolation feature (i) a decrease in precipitation inland of tropical South America due to an anomalous cooling of the South American continent and a weakening of the South American summer monsoon, and (ii) an increase in precipitation in eastern Brazil that is associated with the intensification and southward movement of the Atlantic Intertropical Convergence Zone, which in turn is caused by the strengthening of African winter monsoon that is induced by the anomalous cooling of northern Africa. The cooling of Africa also intensifies and shifts the South Atlantic convergence zone northward by generating a Rossby wave to the west of southern Africa. In times of low insolation, $\delta^{18}O_p$ increases in the northern Andes and decreases in northeastern Brazil, consistent with the pattern of $\delta^{18}O_c$ changes seen in speleothems. Further analysis shows that the decrease in $\delta^{18}O_p$ in northeastern Brazil is due to the "amount

effect"; while the increase in the northern Andes reflects a change in the seasonality of precipitation and in the isotopic composition of vapor that forms the condensate.

TABLE OF CONTENTS

LIST OF FIGURES

LIST OF TABLES

ACKNOWLEDGMENTS

I would like to express my sincerest gratitude to my advisor David Battisti for his extradinary support, patience and guidance through this work. This thesis would not have been completed without all his encouragement and effort. I also offer my sincere gratitude to Chris Bretherton and Dargan Frierson for serving on my supervisory committee and for giving valuable suggestions, encouragement and critique. I always benefit from talking to them. My thanks also go to Qinghua Ding and Gerard Roe, who are always ready to help me and share with me their experiences in doing research.

DEDICATION

To my dear husband, Guozheng Shao.

Chapter 1

INTRODUCTION

In this study, we examine the impact of orbitally forced changes in insolation on the climate and isotopic composition of precipitation over South America. Changes in the Earth's orbit around the Sun cause quasi-periodic changes in insolation reaching the top of the atmosphere. Particularly important for tropical precipitation is precession, with predominant periods at 19,000 and 23,000 years, and the modification to precessional forcing by changes in the eccentricity of the Earth's orbit – hereafter defined as the "precessionally forced" or "orbitally forced" changes in insolation.

The extremely long and well-dated oxygen isotope records stored in the calcite of stalagmites ($\delta^{18}O_c$) renders the precessional cycle an ideal target for understanding the sensitivity of climate and, in particular, the monsoon circulations. Under the right conditions, the $\delta^{18}O_c$ of stalagmites reflects the isotopic composition of the drip water, which reflects the time-integrated oxygen isotope concentration in precipitation, i.e. precipitation-weighted $\delta^{18}O$ (here after, $\delta^{18}O_p$). Figure 1.1 shows the normalized $\delta^{18}O_c$ record of speleothems from South America that are sufficiently long to resolve the precessional cycle (see chapter 2 for details of the speleothem data used in this study). Superposed on each isotope record is the December-January-February mean insolation at 30°S normalized to have the same standard deviation of each record but unitless. The isotope records line up well with the time series of insolation, implying a strong driving force from insolation.

Cruz et al. (2005) examined high-resolution oxygen isotope records in stalagmites from southeastern Brazil. They suggested that the decrease in $\delta^{18}O_c$ during the insolation maxima in Southern Hemisphere summer is due to the southward movement

of South America summer monsoon (SASM), increasing the ratio of summer to winter precipitation ("increased seasonality"), and to the intensified convective activity in the SASM, depleting the heavier isotope in the vapor transported to southern Brazil. Cheng et al. (2013) studied a suite of stalagmites from the eastern flank of the Andes in northern Peru, where in today's climate 80% of the total vapor that forms the precipitation originates upstream over the Amazon Basin. They also suggested that precessional changes in the $\delta^{18}O_c$ of stalagmites primarily reflects changes in the fractionation efficiency of water vapor upstream and hence changes in the strength of SASM. Cruz et al. (2009) studied a 25,000-year long speleothem record from Nordeste, Brazil; they concluded that the precessional signals in the speleothem record indicate changes in the intensity of precipitation during the SASM (misleadingly called the "amount effect").

Although the $\delta^{18}O_c$ of speleothems is a direct measure of the $\delta^{18}O$ of aggregated precipitation ($\delta^{18}O_p$) falling at the cave sites, we cannot directly infer changes in precipitation from the $\delta^{18}O_c$ because the latter is affected by many factors, including: changes in the seasonality of precipitation, changes in the intensity of precipitation (the "amount effect" (Lee and Fung, 2008)), and changes in the isotopic composition of the vapor that is available to form precipitation. We cannot fully address all these factors and thus interpret the climatological significance of the $\delta^{18}O_c$ of speleothems without additional proxy data or the aid of a climate model that incorporates the water isotopes. And only with a climate model can we understand the dynamical processes responsible for the changes in $\delta^{18}O_c$ and climate.

An isotope-enabled GCM is a useful tool to gain some quantitative and comprehensive information about the changes in $\delta^{18}O_c$ and climate and the relationship between the two. In turn, the large amplitude, orbitally paced and accurately dated $\delta^{18}O_c$ oscillations in the cave records provide a good constraint by which we can evaluate the efficacy of a climate model's response to external forcing. Our confidence in the model is enhanced if the simulated $\delta^{18}O_p$ is very close to $\delta^{18}O_c$ of speleothems. In

this study, we examine the impact of orbital forcing (again, defined as the combined effects of precession and eccentricity) on South American climate, with the aid of the isotope-enabled model, ECHAM4.6 (remove "ECHAM4.6", as it is not introduced until chapter 2).

There are three possible ways that orbital forcing can impact the climate of South America: 1) by changing the heating of the Amazon Basin, i.e. changing South American summer monsoon; 2) by changing the heating of Africa; 3) by changing the sea surface temperature (SST) distribution in the Atlantic or/and Pacific oceans. Kutzbach and Guetter (1986) proposed that the orbitally paced insolation strengthens (weakens) the summer monsoon by enhancing (weakening) the land heating. Given the large land area of tropical South America, it is quite likely that orbital forcing directly changes the strength of South American summer monsoon and thus changes the climate and $\delta^{18}O_p$ over tropical South America. On the other hand, Cook et al. (2004) proposed that Africa influences the climate of South America by way of an "intercontinental teleconnection". They found that heating over Africa decreased the precipitation over northeastern Brazil through low-level moisture divergence and dry air advection. Paleoclimate data and archeological evidence have shown that changes in the Earth's orbit pace the climate of Africa (deMenocal and Tierney, 2012). It is therefore possible that orbitally forced changes over Africa affect the climate of South America through an "intercontinental teleconnection". Finally, numerous studies have pointed out that changes in spatial distribution of SST in the tropical Atlantic and Pacific have a profound impact on the climate of tropical South America (Moura and Shukla, 1981; Mechoso et al., 1990; Nobre and Shukla, 1996; Dettinger et al., 2001). For example, Moura and Shukla (1981) proposed that anomalously warm water in the north tropical Atlantic and/or cold water in the south tropical Atlantic are responsible for severe droughts over northeastern Brazil by way of a thermally direct local Hadley circulation response. Hence, it is also possible that insolation-forced changes in the distribution of tropical SST impact the climate of tropical South America.

It is worth noting that these three processes are not mutually exclusive. For any given region, orbitally forced changes in local precipitation may be a result of the combined work of all these three processes. To illuminate the relative importance of these three processes, we will perform a unique set of experiments that are described in detail in chapter 5.

The paper is organized as follows. We describe in chapter 2 the speleothem data, instrumental data, and the climate model that are used in this study, as well as the two core experiments. We also describe the decomposition method for determining the cause(s) of the changes in $\delta^{18}O_p$ simulated by the model. Chapter 3 presents the results from the experiments. Chapter 4 illuminates the causes of the changes in $\delta^{18}O_p$ in the experiments. In chapter 5, we identify the causes of the changes in precipitation. A discussion and conclusion is presented in chapters 6 and 7, respectively.

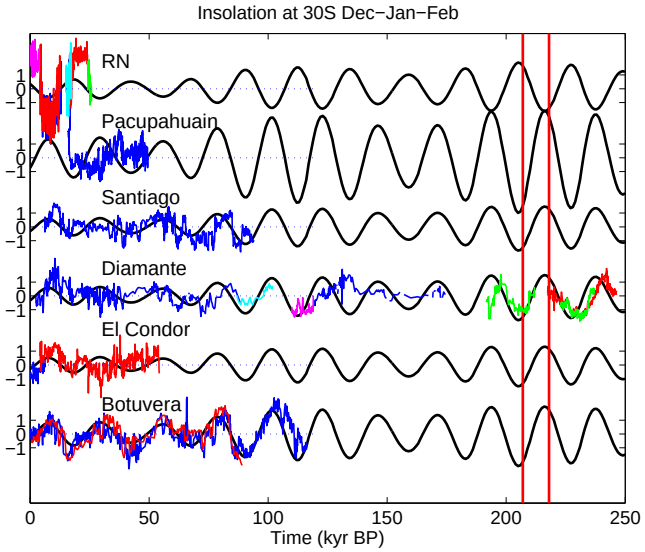

Figure 1.1: Normalized $\delta^{18}O_c$ record of speleothems from South America (color lines), and December-January-Feburary mean insolation at 30°S normalized to have the same but unitless standard deviation as in each record (black line). Different colors for $\delta^{18}O_c$ of a given site represent different speleothems from the same cave. Note that except for Rio Grande do Norte (RN), the insolation is multiplied by -1 for ease in comparison to $\delta^{18}O_c$. The vertical red lines denote the summer insolation used in the high insolation (207 kbp) and low insolation (218 kbp) experiments with ECHAM4.6. Details on the speleothems used can be found in Fig. 2.2 and Table 1.

Chapter 2

DATA, METHODS AND THE CORE EXPERIMENTS

2.1 Experimental Design

The ECHAM atmospheric general circulation model version 4.6 (hereafter ECHAM4.6; Roeckner, 1996) is used in the study. A water isotope module is included in ECHAM4.6 that accounts for the fractionation processes related to evaporation and condensation (more details can be found in Hoffmann et al. (1998)). The model is run in T42 resolution with 19 vertical levels, and is coupled to a 50 m slab ocean. A cyclostationary heat flux (q-flux) is added to the slab ocean to account for ocean heat flux convergence by ocean currents and for biases in the surface heat flux due to biases in the atmospheric model. The q-flux is constructed by a three-step process: first, the observational climatological mean SST is used to force ECHAM4.6; then the surface flux output from AGCM is used to force the uncoupled (offline) slab ocean; finally, the differences between the SST output from the offline slab ocean simulation and the observed SST are used to construct the cyclostationary heat flux that is added to the freely evolving coupled model.

We performed two core experiments with ECHAM4.6 to quantitatively study the effect of orbital forcing on climate and the isotopic composition of precipitation in South America. In the first experiment, called the high insolation experiment, we used the insolation value of 207,000 years before present (207 kbp). In the second experiment, called the low insolation experiment, insolation of 218 kbp is used. Insolation of these two years represents respectively the minimum and maximum of northern hemisphere (NH) summer insolation over the past 950,000 years. These two years are also years of near-maximum and near-minimum summer insolation of the

southern hemisphere (SH), respectively. Figure 2.1 shows the differences in insolation between low insolation and high insolation experiments. Compared with the high insolation experiment, the low insolation experiment has more insolation in June, July and August, but less insolation in December, January and Feburary (DJF). This insolation deficit in DJF peaks in the high latitudes of SH, but extends northward to 60°N.

The same boundary conditions (360ppm CO_2 and modern day continental geometry, orography and ice sheets) and the same climatological seasonal cycle of heat flux are used in both experiments: in effect, we do not take into account any changes in ocean heat flux convergence that would arise due to changes in the ocean advection or mixing. All experiments discussed in this study are run for 30 years, with output of the last 20 years used to construct climatologies and climatological differences; all differences discussed in this paper are statistically significant at $p = 0.05$ or better.

2.2 Proxy Data

The speleothem data we used to evaluate the model's performance were obtained from the NOAA Paleoclimatology website (http://www.ncdc.noaa.gov/paleo/speleothem.html). Figure 2.2 shows sites of the caves where the speleothems are from: Rio Grande do Norte in northeastern Brazil (Cruz et al., 2009), El Condor and Cueva del Diamante in northern Peru (Cheng et al., 2013), Santiago in Ecuador (Mosblech et al., 2012), Pacupahuain cave in Peru (Kanner et al., 2012) and Botuverá in southern Brazil (Cruz et al., 2005; Wang et al., 2007). These caves concentrate around three regions of South America: along the eastern flank of the Andes, in northeastern Brazil and in southeastern Brazil.

Also shown in Fig. 2.2 is the modern day climatological precipitation for DJF, using monthly Climate Prediction Center (CPC) Merged Analysis of Precipitation (CMAP) data (Xie and Arkin, 1997), from January 1979 to December 2010. These data are available at http://www.esrl.noaa.gov/psd/data/gridded/data.cmap.html.

Three precipitation centers can be identified in Fig. 2.2: a narrow zonally oriented band over the tropical North Atlantic Ocean, a broad region over continental South America, and a broad northwest-southeast oriented band over the subtropical Atlantic Ocean. The narrow tropical rain band over the ocean is called the Atlantic Intertropical Convergence Zone (ITCZ), and denotes the convergence of the Trade Winds from both hemispheres. It migrates north-south with the seasonal cycle of insolation, but stays north of the equator all year around (Philander et al., 1996; Waliser and Gautier, 1993). The broad region of precipitation over continental South America is associated with convection over Amazonia in austral summer. Due to the low thermal inertia of land, this broad center of precipitation exhibits a prominent seasonal cycle, migrating from around the equator in austral winter to as far south as 25°S in austral summer (Fig. 2.2). This seasonal dependence has led some scientists to describe it as Monsoon-like, calling it South American summer monsoon (SASM; Zhou and Lau, 1998; Vera et al., 2006). The subtropical rainband, known as South Atlantic Convergence Zone (SACZ) is due to both the passage of extratropical transient frontal systems and to mean low-level convergence. It weakly migrates northward from austral winter to austral summer (Kodama, 1993). A detailed discussion of these mean field features can be found in Garreaud et al. (2009).

From a climate perspective, caves in the northern Andes are at the western edge of SASM. Hence, speleothems from these caves are affected by changes in the SASM, including the seasonal migration and strengthening/weakening of the SASM. The cave site in northeastern Brazil is influenced in austral summer by the westernmost tail of the ITCZ, and the easternmost edge of the SASM; it records changes in both ITCZ and SASM. The cave site in southern Brazil is on the border between SASM and SACZ, so it records climate changes in the SACZ as well as the SASM.

2.3 Decomposition Method

The precipitation-weighted $\delta^{18}O$ ($\delta^{18}O_p$) is defined as $\frac{\sum_j \delta^{18}O_j \cdot P_j}{\sum_j P_j}$, where $\delta^{18}O_j$ is monthly isotopic composition of precipitation ($\delta^{18}O$), and P_j is monthly precipitation [1]. Thus, the difference in $\delta^{18}O_p$ between the low insolation and high insolation experiment is

$$\delta^{18}O_{p_{218}} - \delta^{18}O_{p_{207}} = \frac{\sum_j \delta^{18}O_{j,218} \cdot P_{j,218}}{\sum_j P_{j,218}} - \frac{\sum_j \delta^{18}O_{j,207} \cdot P_{j,207}}{\sum_j P_{j,207}} . \quad (2.1)$$

Changes in $\delta^{18}O_p$ may result from changes in several local or nonlocal processes. To quantitatively address all possible factors, we decompose the total changes in $\delta^{18}O_p$ into two parts: 1) those due to changes in the amount of monthly precipitation, and 2) those due to changes in the monthly isotopic composition of precipitation; the latter may be due to changes in precipitation intensity or to changes in the isotopic composition of the water vapor that is condensed to form the precipitate.

The importance of changes in the seasonality of precipitation to the changes in $\delta^{18}O_p$ is indicated by

$$\frac{\sum_j \delta^{18}O_{j,207} \cdot P_{j,218}}{\sum_j P_{j,218}} - \frac{\sum_j \delta^{18}O_{j,207} \cdot P_{j,207}}{\sum_j P_{j,207}} . \quad (2.2)$$

The importance of changes in $\delta^{18}O$ of precipitation to the changes in total $\delta^{18}O_p$ is indicated by

$$\frac{\sum_j \delta^{18}O_{j,218} \cdot P_{j,207}}{\sum_j P_{j,207}} - \frac{\sum_j \delta^{18}O_{j,207} \cdot P_{j,207}}{\sum_j P_{j,207}} . \quad (2.3)$$

It is worth noting that the results from Eq. 2.2 and Eq. 2.3 do not sum to the total changes in $\delta^{18}O_p$ (Eq. 2.1) because of the inherent nonlinearity in the definition of

[1] The traditional definition of the climatological $\delta^{18}O$ features the ratio of the moles of ^{18}O molecules to the moles of ^{16}O molecules. The precipitation weighted formulation $\delta^{18}O_p$ is an excellent approximation of the climatological $\delta^{18}O$ (errors of $\mathcal{O}(0.2\ \%)$; see Battisti et al. (2014)) that provides additional insight on the processes and seasonality that contribute to the climatological $\delta^{18}O$.

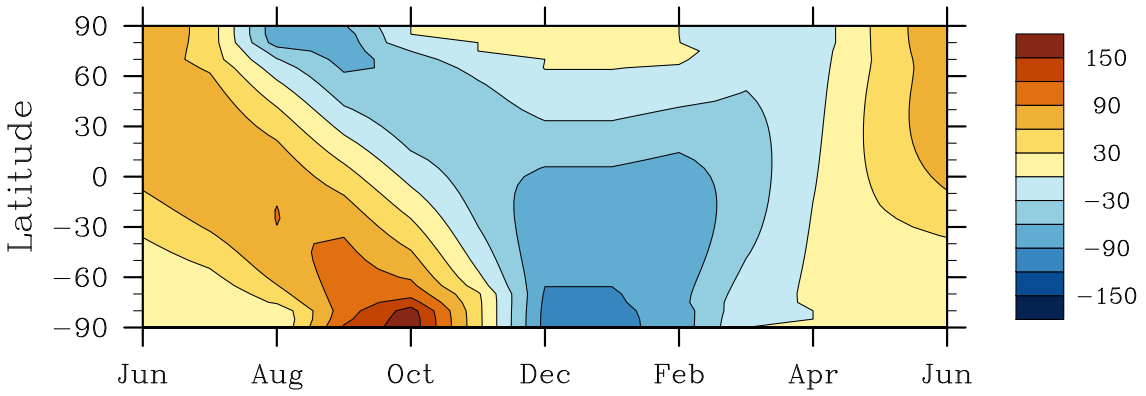

Figure 2.1: The difference in insolation at the top of the atmosphere, low insolation minus high insolation (218 kbp minus 207 kbp). Units are Wm^{-2}.

$\delta^{18}O_p$.

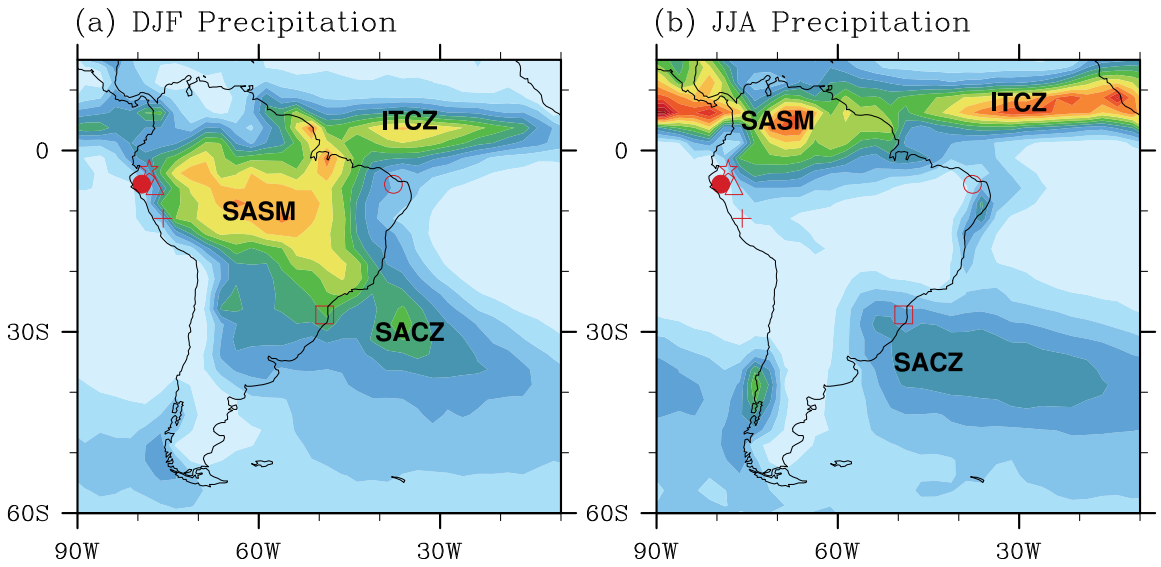

Figure 2.2: The observed climatological DJF precipitation (shading; data are from monthly Climate Prediction Center (CPC) Merged Analysis of Precipitation (CMAP) data). The location of the speleothems used in this study are denoted in red: ☆-Santiago, △-El Condor,●-Cueva del Diamante, ✝-Pacupahuain Cave, ◯-Rio Grande do Norte, □- Botuverá cave. Cueva del Diamante is almost at the same location as El Condor, and is plotted offset by two degrees to the east to make both distinguishable. Units of precipitation are mm/day.

Table 2.1: Speleothems used in this study and featured in Figs. 1.1, 2.2 and 3.1. For each record, we note the cave location, elevation above sea level, the duration of the record and the reference for the data. Also noted is the amplitue of the precessional cycle. The amplitude of the precessional cycle is found by a linear regression of the measured $\delta^{18}O_c$ against DJF 30°S insolation and then scaled by the difference in insolation 218 kbp minus 207 kbp (which is 90 Wm^{-2}); the 95% confidence interval is noted in parenthesis. The amplitude of the precessional cycle is noted only if the $\delta^{18}O_c$ is correlated with DJF Southern Hemisphere insolation at $p \leq 0.05$.

Cave and Location	Duration	Amplitude	Reference
Rio Grande do Norte (10°10"S, 40°50"W, 500m asl)	24 kyr		Cruz et al. (2009)
Pacupahuain (11°14"S, 75°49"W, 3800m asl)	32 kyr		Kanner et al. (2012)
Santiago (3°1"S, 78°8"W, 980m asl)	86 kyr		Mosblech et al. (2012)
Cueva del Diamante (5°44"S, 77°30"W, 960m asl)	243 kyr	1.0‰(0.2, 1.6)	Cheng et al. (2013)
El Condor (5°56"S, 77°18"W, 860m asl)	53 kyr		Cheng et al. (2013)
Botuvera (27°13"S, 49°10"W, 230m asl)	116 kyr	3.3‰(1.9, 4.2)	Cruz et al. (2005); Wang et al. (2007)

Chapter 3

RESULTS

The differences in $\delta^{18}O_p$ between the low insolation and high insolation experiments (low insolation minus high insolation) are displayed in Fig. 3.1.[1] Also plotted in Fig. 3.1 are the estimates of the differences in $\delta^{18}O_c$ from the speleothems, linearly scaled by the difference in summer insolation, 218 kbp minus 207 kbp. Our experiments were performed using the extreme values of summer insolation, last realized 218 and 207 thousand years ago. The cave records do not extend this far back. Hence, we estimate the differences in $\delta^{18}O_c$ at the cave sites between 218 kbp and 207 kbp using linear fit of the $\delta^{18}O_c$ of speleothems to the 30°S DJF insolation, and then scale the regression value to reflect the changes in DJF insolation between 218 kbp and 207 kbp (90 W/m^2). The scaled differences in $\delta^{18}O_c$ between 218 kbp and 207 kbp are: +3 ‰ at Botuverá in southeastern Brazil, and +1 ‰ at Diamante cave in the northern Andes. Records from the other three sites are too short to have a statistically significant (at $p = 0.05$) correlation with insolation. The model captures the gross dipole pattern indicated by the cave $\delta^{18}O_c$. It also gives the same quantitative estimates over the northern Andes. Over southeastern South America, the model underestimates the $\delta^{18}O_c$ change. The pattern of our simulated changes in $\delta^{18}O_p$ agrees with that of Cruz et al. (2009), who use the same GCM driven by modern sea surface temperature, but set the insolation forcing to be 6 kbp and 0 kbp, respectively, which are also minima and maxima of DJF insolation, but of smaller amplitudes.

Figure 3.2a shows the differences in precipitation; superposed in contours is the

[1] Unless otherwise noted, "differences" discussed in the paper and plotted in the figures will always refer to low insolation minus high insolation.

DJF mean precipitation of the high insolation experiment. Compared to the high insolation experiment, precipitation in low insolation experiment decreases by over 1mm/day over the SASM region, indicating a weakening of summer monsoon. Precipitation increases greatly in an arc along the eastern coast of Brazil and offshore over the ocean, where the DJF mean precipitation increases from 5 mm/day in the high insolation experiment to over 13 mm/day, indicating a southward shift and intensification of the ITCZ and an intensification and northward shift of the SACZ. This northward shift of SACZ and southward shift of ITCZ constitues a shrinking of the dry zone that is formed due to the large-scale mid-tropospheric subsidence associated with the South Atlantic High. Curiously, this kind of dry zone shrinking is also seen in the Pacific when El Niño happens (Yulaeva and Wallace, 1994).

Figure 3.2b shows differences in temperature between the low insolation and high insolation experiments. The decrease in precipitation in the Amazon basin is accompanied by a slight warming, whereas the increase in precipitation in the eastern Brazil is accompanied by a large cooling (by over 3K). South of the SACZ, the decrease in precipitation again is accompanied by an increase in tempreature (by over 1K). These changes in temperature are consistent with the changes in clouds that are associated with changes in precipitation: the decrease in precipitation over monsoon region in the central Amazon is associated with fewer clouds and therefore more incoming solar radiation, which more than offsets the cooling caused by decrease in local summer insolation. Similarly, more precipitation over the eastern Brazil is associated with more clouds and thus less incoming solar radiation, which adds to the orbitally-induced cooling and makes the surface air temperature even lower.

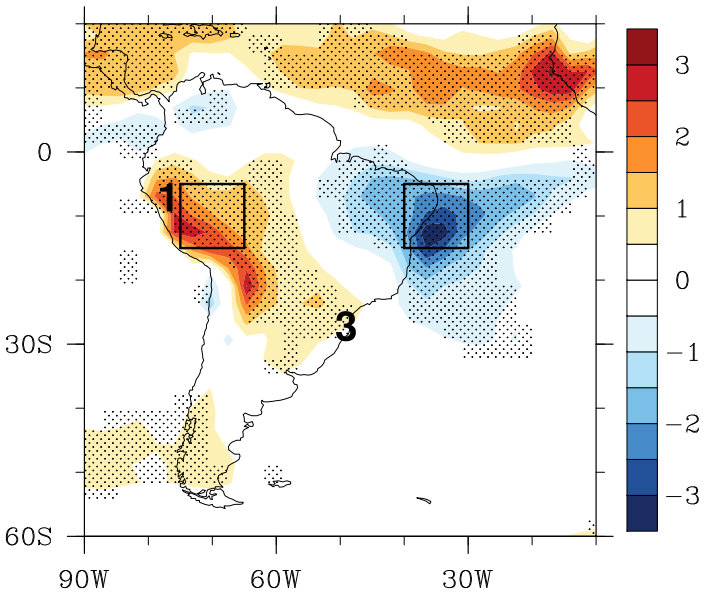

Figure 3.1: Difference in $\delta^{18}O_p$ between the low insolation and high insolation experiment. Numbers are the scaled estimates of the changes in the $\delta^{18}O_c$ from speleothems (see chapter 2); only records whose correlation coefficents with insolation are statistically significant at $p = 0.05$ are noted. Stippling indicates regions where the difference in simulated $\delta^{18}O_p$ is statistically significant from zero at a significance level of 0.05. Boxes represent regions over which domain averages are examined in chapter 4.

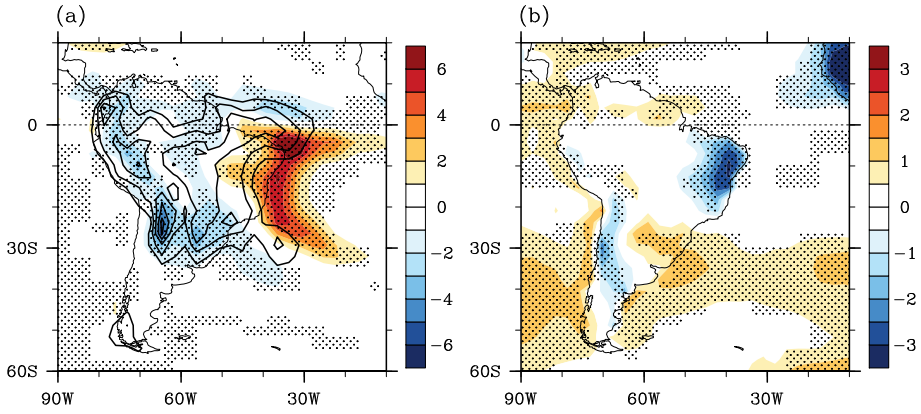

Figure 3.2: Difference in DJF precipitation (a) and surface air temperature (b) between the low insolation and high insolation experiment (units are Kelvin and mm/day, respectively). Also shown in contours in the left panel is the climatological DJF precipitation in the high insolation experiment (207 kbp); contours start from 4 mm/day; contour interval is 2 mm/day. Stippling is as in Fig. 3.1.

Chapter 4

ANALYSIS ON ISOTOPIC RESPONSES

The decomposition method shown in Eqs. 2.2 and 2.3 is used to quantitatively illuminate the reason for changes in $\delta^{18}O_p$. Using the monthly $\delta^{18}O$ from high insolation, and the monthly precipitation of low insolation in the calculation of $\delta^{18}O_{p_{218}}$ (Eq. 2.2), we isolate the differences in $\delta^{18}O_p$ caused by changes in the seasonality of precipitation; the result is displayed in Fig. 4.1c. Similarly, using the monthly precipitation from high insolation, and the monthly $\delta^{18}O$ from low insolation, we calculate the contribution of the changes in the isotopic composition of precipitation to the changes in $\delta^{18}O_p$ (Fig. 4.1d). Comparing Figs. 4.1c, d with 4.1a, we see that over the northern Andes changes in both $\delta^{18}O$ and the seasonality of precipitation contribute to the total change in $\delta^{18}O_p$. However, over the northeastern Brazil, the change in $\delta^{18}O_p$ is largely due to the change in the $\delta^{18}O$ of precipitation.

We apply a similar decomposition method to examine the relative contribution of winter and summer changes in precipitation and $\delta^{18}O$ to the change in $\delta^{18}O_p$. Specifically, in the calculation of $\delta^{18}O_{p_{218}}$, we use the monthly precipitation and $\delta^{18}O$ values in DJF from low insolation experiment, and the values from high insolation experiment for all the other months. The differences between this partial $\delta^{18}O_p$ and $\delta^{18}O_{p_{207}}$ are displayed in Fig. 4.1b. Over the northern Andes, the change in $\delta^{18}O_p$ is seen to be due to changes in both DJF and other seasons (cf Figs. 4.1a and b) and involves changes in both the precipitation and the $\delta^{18}O$ of precipitation. Over the northeastern Brazil, almost all the change in $\delta^{18}O_p$ is due to changes in the $\delta^{18}O$ of the summertime (DJF) precipitation (cf Figs. 4.1a and b; see also chapter 4a).

4.1 Change in $\delta^{18}O_p$ over the northeastern Brazil

The above results can be further understood by examining the seasonal cycle of precipitation and the $\delta^{18}O$ of precipitation in the low insolation and high insolation experiments. Figures 4.2a,c display the seasonal cycles of the area-averaged precipitation and $\delta^{18}O$ of precipitation over the northeastern Brazil. The region used to calculate the area average is shown in Fig. 3.1. Compared with the high insolation experiment, the low insolation experiment has much more precipitation in DJF, but almost the same amount in JJA. More precipitation in DJF in low insolation experiment has little effect on the precipitation-weighted $\delta^{18}O$, however, because there is little precipitation in winter compared to summer; hence, changes in the amount of summer precipitation do not effect the seasonality of precipitation. This is consistent with the decomposition analysis shown in Fig. 4.1a and 4.1c: changes in the seasonality of precipitation contribute little to the total change in $\delta^{18}O_p$ over northeastern Brazil. Figure 4.2c shows that there is a large decrease in $\delta^{18}O$ of precipitation in DJF of the low insolation experiment; this accounts for the majority of the changes in $\delta^{18}O_p$ because the bulk of the annual precipitation occurs in DJF in both the low insolation and high insolation simulations. Finally, to determine why the $\delta^{18}O$ of summertime precipitation changes, we calculate the cumulative probability distribution function (cdf) for daily precipitation over northeastern Brazil (Fig. 4.3a,c). The region used in this calculation is same as the one shown in Fig. 3.1. The intensity of precipitation changes very little in JJA. In DJF, however, corresponding to the more negative $\delta^{18}O$, a greater fraction of precipitation is falling as heavy precipitation in low insolation compared to high insolation. This out-of-phase relationship between changes in the intensity of precipitation and changes in $\delta^{18}O$ of precipitation suggests that the "amount effect" (Lee and Fung, 2008) is acting to deplete the $\delta^{18}O$ of precipitation in northeastern Brazil in DJF in the low insolation experiment relative to the high insolation experiment.

The more intense precipitation in DJF over northeastern Brazil is due to an increase in moist static energy (MSE). Figure 4.4a shows the differences in MSE for DJF. Compared to high insolation, in the low insolation experiment, MSE increases south of the equator, including over northeastern Brazil, and decreases north of the equator over tropical Atlantic, consistent with the southward movement of ITCZ (Fig. 3.2).

Therefore, we can conclude that the decrease in the precipitation-weighted $\delta^{18}O$ ($\delta^{18}O_p$) over northeastern Brazil in low insolation compared to high insolation is due to a decrease in the $\delta^{18}O$ of precipitation in summer, which appears to be due to an increase in the intensity of precipitation associated with a southward shift of ITCZ. The cause of this southward shift of ITCZ will be discussed in chapter 5.

4.2 Change in $\delta^{18}O_p$ along the Andes

In this chapter, we perform the same analysis as in chapter 44.1, only for the northern Andes region. Figure 4.2b shows that low insolation has less precipitation than high insolation in the wet season (DJF), but more precipitation than high insolation in the dry season (JJA). Thus, a larger portion of annual precipitation in low insolation comes in the dry season. The weakening of seasonality of precipitation contributes to a higher $\delta^{18}O_p$ in low insolation experiment because the $\delta^{18}O$ of precipitation is more depleted in DJF compared to JJA in both the low insolation and high insolation experiments (Fig. 4.2d). Compared to high insolation, $\delta^{18}O$ of precipitation in low insolation also increases in DJF but changes very little in JJA (Fig. 4.2d). Since DJF is the wet season in both the low insolation and high insolation experiments, this change in DJF $\delta^{18}O$ also contributes significantly to the precessional changes in $\delta^{18}O_p$. Hence, unlike in northeastern Brazil, in the northern Andes, changes in both the seasonality of precipitation and the $\delta^{18}O$ of precipitation contribute to the net change in $\delta^{18}O_p$. This is consistent with the decomposition analysis result shown in Figs. 4.1c and d.

Figures 4.3b, d show the cumulative probability distribution function (cdf) for

daily precipitation over the northern Andes. For JJA, daily precipitation is more intense in low insolation experiment than in high insolation experiment – as evidenced from the cumulative probability distribution of precipitation (Fig. 4.3b) and the changes in moist static energy (Fig. 4.4b). This suggests that the vapor condensed on site to form precipitation must be heavier to offset the decrease in $\delta^{18}O$ associated with more intense precipitation. In DJF, the intensity of daily precipitation changes very little, but the $\delta^{18}O$ of precipitation increases a lot. Thus, the "amount effect" cannot account for the simulated changes in $\delta^{18}O$ in DJF. Less precipitation, coupled with very little change in the distribution of intensity, implies the decrease in precipitation in DJF is due to a uniform reduction in the frequency of all types of precipitation; convection strength changes little. Thus, the heavier $\delta^{18}O$ of the precipitation in DJF is due to heavier vapor imported into the region from the east, which is associated with the reduced intensity of the SASM (Fig. 3.2).

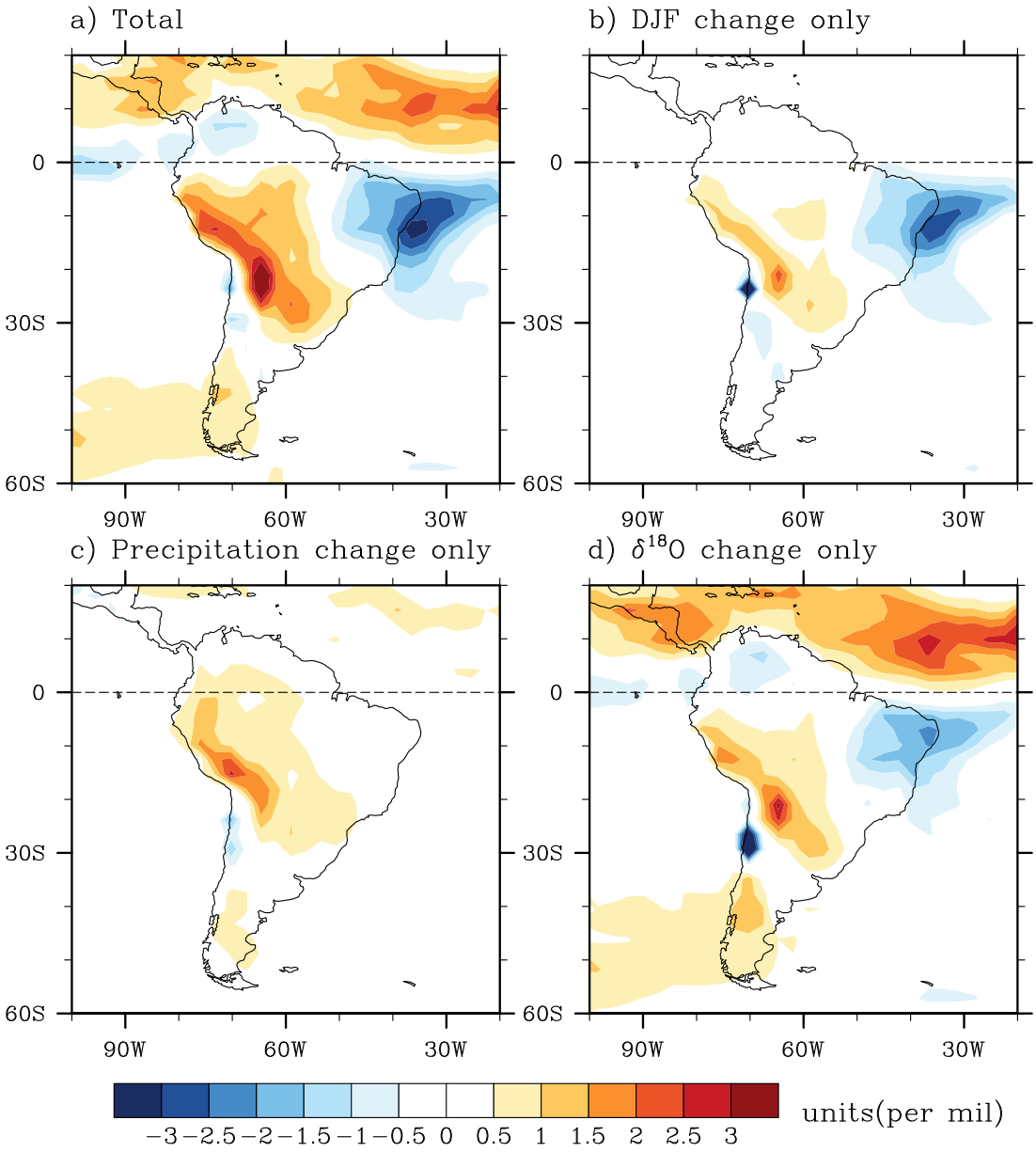

Figure 4.1: Difference in $\delta^{18}O_p$, low insolation minus high insolation experiment from ECHAM4.6 (a). Panel (b) shows changes in $\delta^{18}O_p$ due solely to changes in DJF precipitation and $\delta^{18}O$. Changes in $\delta^{18}O_p$ due solely to changes in the annual cycle of precipitation (Eq. 2.2) and solely to changes in the annual cycle of $\delta^{18}O$ of precipitation (Eq. 2.3) are shown in panels (c) and (d), respectively.

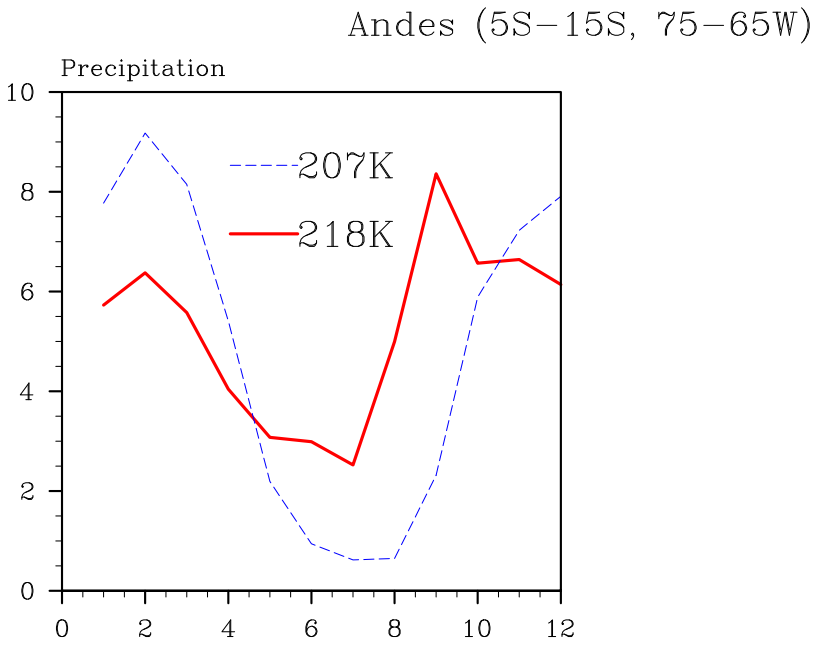

Figure 4.2: Area-averaged precipitation (a) and $\delta^{18}O$ (c) in the northeastern Brazil (5°S-15°S, 40°W-30°W) in the high insolation (blue) and low insolation (red) experiments. (b) and (d) are same as (a) and (c), but for the eastern flank of the Andes (5°S-15°S, 75°W-65°W).

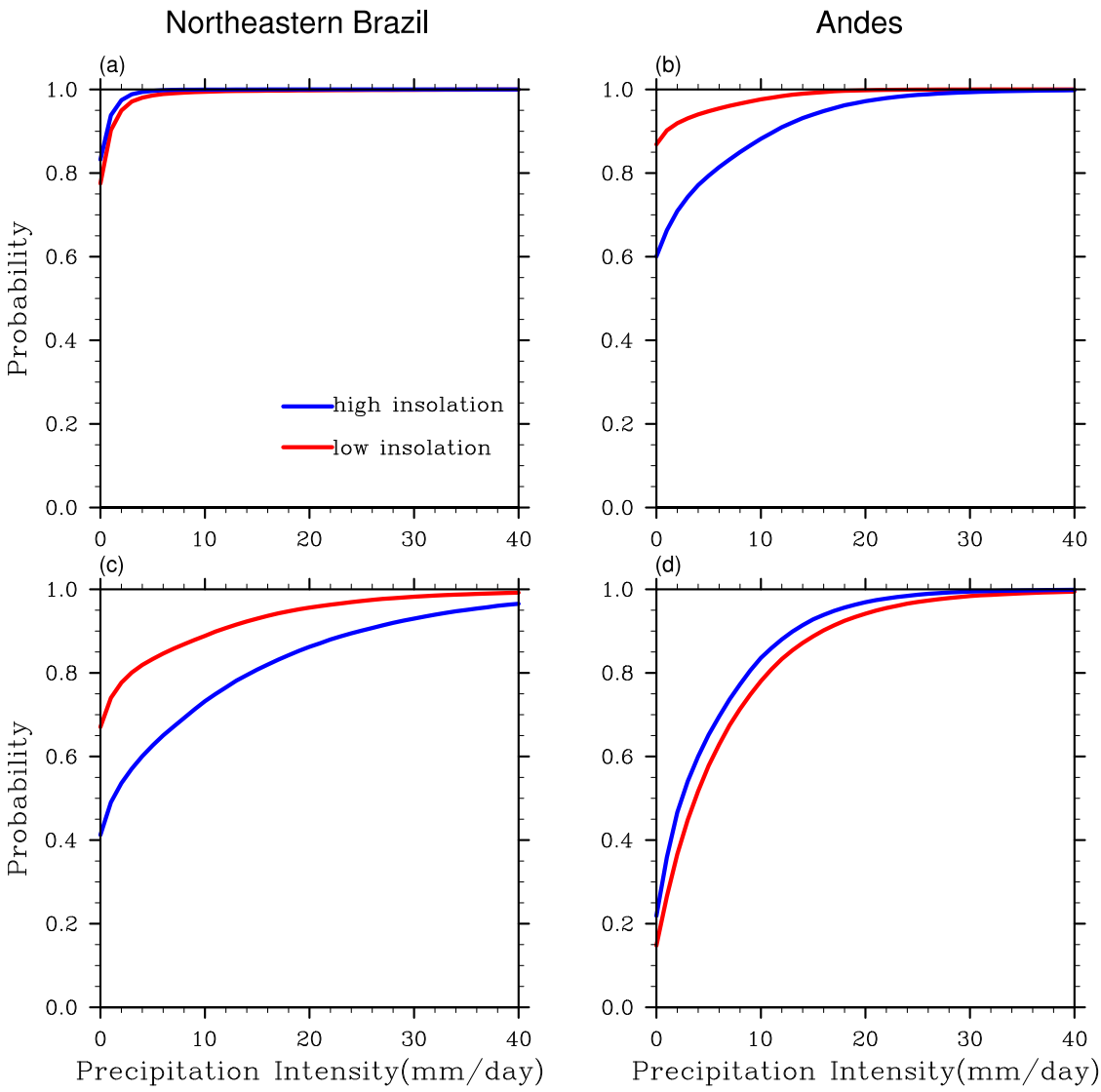

Figure 4.3: Cumulative probability distribution of daily precipitation for the northeastern Brazil (a and c) and northern Andes (b and d) in the high insolation (blue) and low insolation (red) experiments in austral winter (JJA, upper panels) and austral summer (DJF, lower panels).

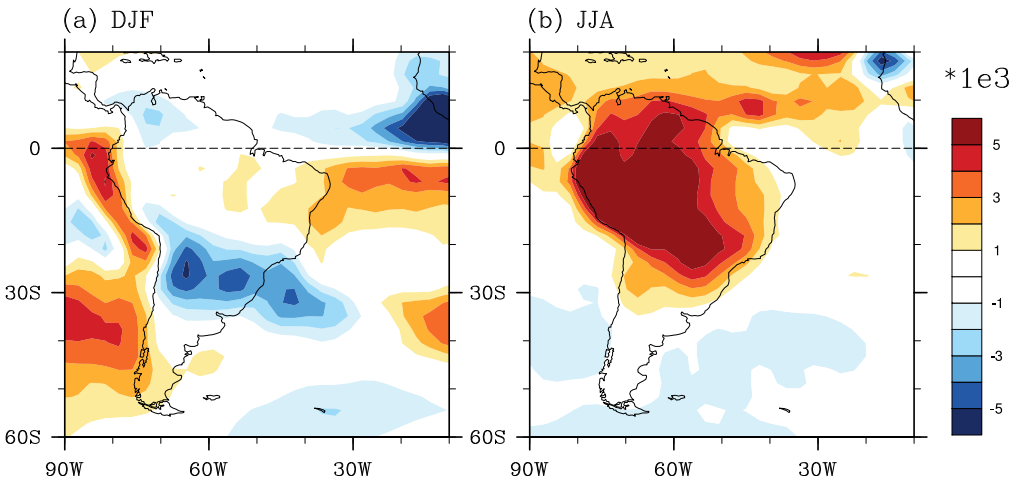

Figure 4.4: Difference in moist static energy between the low insolation and the high insolation experiments for (a) DJF and (b) JJA. Units are J/kg.

Chapter 5

ANALYSIS OF THE CLIMATE CHANGES

5.1 The relative roles of insolation forcing of South America, Africa and the oceans

To identify the essential processes that cause the orbitally induced changes in precipitation, we have performed a series of experiments that isolate the impact of the changes in insolation in selected regions: tropical South America, Northern Africa and Southern Africa. Since changing local insolation would require significant recoding of the model, we approximate the changes in local insolation forcing by changing the local surface albedo. Starting from the boundary conditions of the high insolation experiment, we mimic the changes in the local absorption of insolation in DJF in the low insolation experiment by increasing the surface albedo by a factor of 2.5 (the estimate of the appropriate scaling factor is presented in the appendix). These experiments are not perfect analogs to the local DJF forcing in the low insolation experiment, however, because there are differences in the vertical distribution of forcing changes, and because changing the surface albedo gives a year-around reduction in shortwave forcing whereas orbital forcing decreases the DJF insolation while increasing the springtime heating in the Southern Hemisphere. Nonetheless, so long as we focus on the SH summer season and changes in SST are not important (see chapter 55.15.1.3 below and Fig. 5.2), the differences in the sign of forcing in JJA has little effect on the DJF response, and the response to the "increasing albedo" experiments serves as a reasonable proxy for the response to the low insolation forcing in DJF because land has a sufficiently low heat capacity.

We first perform two fixed SST experiments to make sure that the fixed SST

experiments reproduce closely the slab ocean experiments. In the first experiment, called "highInsolation_highSST", we use insolation and SST output of the high insolation simulation. In the second experiment, we use insolation and SST output of the low insolation simulation. As expected, the difference in precipitation (and isotopes) between these two experiments is nearly identical to the difference between the low insolation and high insolation experiments using the slab model.

The highInsolation_highSST experiment thus serves as the reference experiment for all of the "increasing albedo" experiments discussed below. These three experiments are: increasing surface albedo by a factor of 2.5 (i) over South America only, (ii) over Africa only, and (iii) over both South America and Africa. These three experiments are called the "2.5x South America alone", "2.5x Africa alone" and "2.5x both South America and Africa" experiments, respectively. These experiments isolate the impact of DJF insolation changes over specific regions on the climate and isotopic composition of precipitation in South America.

5.1.1 Role of South America

Figure 5.1b shows the difference in precipitation between 2.5x South America alone and highInsolation_highSST experiments. Keeping in mind that increasing albedo by a factor of 2.5 does not give exactly the same forcing as in the low insolation experiment, we focus our discussion on the gross spatial pattern of the changes and not the detailed changes. Increasing albedo over South America decreases precipitation over all of the South American continent north of 40°S, as well as over the subtropical ocean south of the climatological mean SACZ. It also slightly increases precipitation over the tropical North Atlantic and to the north of SACZ. Compared with the differences between low insolation and high insolation experiments (Fig. 5.1a), increasing albedo over South America alone reproduces the decreases of precipitation over tropical and subtropical South America and the Andes (SASM), and weakly reproduces the northward shift of SACZ. However, it does not account for the increases in precipitation

along and offshore of the eastern coast of Brazil. It also tends to move ITCZ to the north, whereas ITCZ is shifted southward in the low insolation phase compared to the high insolation phase (low insolation minus high insolation experiments).

Therefore, the weakening of SASM in low insolation experiment is related to weakening of the heating of South American continent, which is caused by a reduction of insolation in the low insolation experiment. These changes in the SASM are reflected in the changes in subcloud moist static energy (Fig. 4.4a). This weakening of land heating significantly cools the troposphere, lowers the moist static energy, and decreases the monsoon convection intensity.

5.1.2 Role of Africa

Figure 5.1c shows that increasing albedo over Africa alone reproduces the precipitation increase along the eastern coast of Brazil and south of the equator over tropical Atlantic (cf Fig. 5.1a and c). It also reproduces the northward shift and intensification of SACZ. However, it doesn't reproduce the precipitation decreases seen north of 20°S over the South American continent. Also worth noting is that the 2.5x Africa alone experiment reproduces the basin-wide southward shift of the tropical Atlantic ITCZ. This implies that independent of any changes in SST, cooling over Africa is an important driver for the orbitally driven shift of ITCZ in the Atlantic and the changes in the SACZ.

Increasing the surface albedo over both continents basically reproduces the precipitation changes over the whole South America, as well as the shifts in the ITCZ and SACZ (cf Figs. 5.1a and d). The precipitation changes that result from increasing albedo over both Africa and South America are very similar to the sum of the precipitation changes from the experiment where the albedo is increased over each continent seperately: the result in Fig. 5.1d is very close to the sum of Fig. 5.1b and Fig. 5.1c. In other words, the response is nearly linear.

5.1.3 Role of Ocean Temperature Change

The only discrepancy between the orbitally forced DJF precipitation changes (Fig. 5.1a) and those due to the changes in albedo over both South America and Africa (Fig. 5.1d)) is just north of the equator in the Atlantic ocean. This is demonstrated by performing one additional experiment with ECHAM4.6. In this experiment, called "highInsolation_lowSST", we use high insolation, but SST from low insolation experiment. The differences in precipitation between this experiment and the highInsolation_highSST experiment are then due to differences in SST only, and are shown in Fig. 5.2a. Note that the SST differences are due to both differences in *in situ* insolation and to enhanced cold air advection by the mean northeasterly Trade Winds associated with the anomalously cool Sahara in DJF (due to a deficit in insolation in low insolation compared to high insolation experiment).

The differences in precipitation due to insolation-induced changes in SST are confined to a small region northeast of Brazil. Hence, drawing from the results of chapters 5a1 and 5a2 , we conclude that orbitally forced changes in precipitation over South America (and Africa) are caused solely by changes in the heating of land.

To sum up, we conclude that insolation impacts the summer precipitation over South America through two processes: 1) an insoation deficit that directly weakens the South American summer monsoon and decreases precipitation throughout inland South America by decreasing the land heating of South America (thus reducing the moist static enegy that drives convection in the SASM); and 2) an insolation deficit that weakens the heating of Africa, which indirectly increases the precipitation over the eastern edge of South America via teleconnected atmospheric changes (see below). The influence of ocean changes is very small and limited to a small oceanic region north of Brazil.

5.2 How does Africa influence South Amerian climate?

The experiments in chapter 5a demonstrate that the changes in precipitation along the eastern coast and offshore of Brazil are mainly due to changes in the heating of Africa. Cook et al. (2004) added the entire African continent to an aqua planet model and studied the influence of Africa on precipitation to the west of Africa. They concluded that Africa influences the climate of South America through a local Walker circulation response to the heating of southern Africa in January. In this chapter, we perform additional experiments to illuminate the relative importance of insolation changes over southern and northern Africa. We do this by proxy – first increasing the surface albedo of northern Africa by a factor of 2.5, and then increasing the albedo of southern Africa by a factor of 2.5; in both experiments, the SST is prescribed to be that from the high insolation slab experiment. Results are then compared to those from the reference experiment, highInsolation_highSST. Results are shown in Fig. 5.3 and discussed below.

5.2.1 Role of Northern Africa

Figure 5.3a shows the differences in precipitation between 2.5x northern African alone and the control run (highInsolation_highSST experiment). Increasing albedo over northern Africa alone intensifies and shifts the tropical Atlantic ITCZ southward; it has no influence on precipitation along the eastern coast of South America. Figure 5.4b shows the differences in the winds at 925mb. To assist the interpretation of these differences, we also show in Fig. 5.4a the DJF mean winds from the control run (highInsolation_highSST). In the control run, northeasterlies associated with the north African winter monsoon dominate the circulation of northern Africa. These northeasterlies reach as far south as 5°N. Increasing albedo over northern Africa strengthens the northeasterlies, which now reach across the equator to 5°S" (Fig. 5.4b). This strengthening of winter monsoon shifts the ITCZ southward

throughout the tropical Atlantic, increases the precipitation intensity in the eastern tropical Atlantic ITCZ, and hence decreases the precipitation-weighted $\delta^{18}O$ ($\delta^{18}O_p$) over the northeastern Brazil.

5.2.2 Role of Southern Africa

Increasing the albedo of southern Africa causes an increases in precipitation over eastern Brazil; it is also responsible for the intensification and northward shift in the SACZ that are seen in the differences between low insolation and high insolation experiments (cf Figs. 5.3b and 5.1a). It is also responsible for changes in precipitation over southern Africa, which reduces the local condensational heating of the troposphere and gives rise to an anticyclonic Rossby wave to the west (Gill, 1980). As shown in Fig. 5.4c, this anticyclone extends all the way to the eastern coast of South America. The low-level convergence associated with this Rossby wave is predominantly due to the zonal flow ($\partial u/\partial x$) near the equator and meridional flow ($\partial v/\partial y$) in the subtropics. Hence, the anomalous easterlies along the northern branch of the anticyclone converge near northeastern Brazil, contributing slightly to the increase in precipitation just offshore. The northerlies along the western branch of the anticyclone give rise to anomalous convergence in the vicinity of the SACZ and thus enhance the mean moisture convergence (not shown) and increase the precipitation in the SACZ.

The increase in precipition in the SACZ in the low insolation experiment may also result from an increase in eddy activity aloft which is in turn, due to the changes in the upper level flow. Figure 5.5 shows the DJF zonal winds at 200mb. The major difference between the low insolation and high insolation experiments is that the easterlies aloft over the equatorial Atlantic seen in the high insolation experiment are replaced by westerlies. Comparing the other panels in Fig. 5.5 with the low insolation and high insolation panels, we see that the switch from easterlies to westerlies is uniquely associated with the cooling of southern Africa. The shift from easterlies

to westerlies allows more upper level eddies to enter the subtropical region and thus enhances the stochastic stirring of the air below, resulting in an increased likelihood of precipitation.

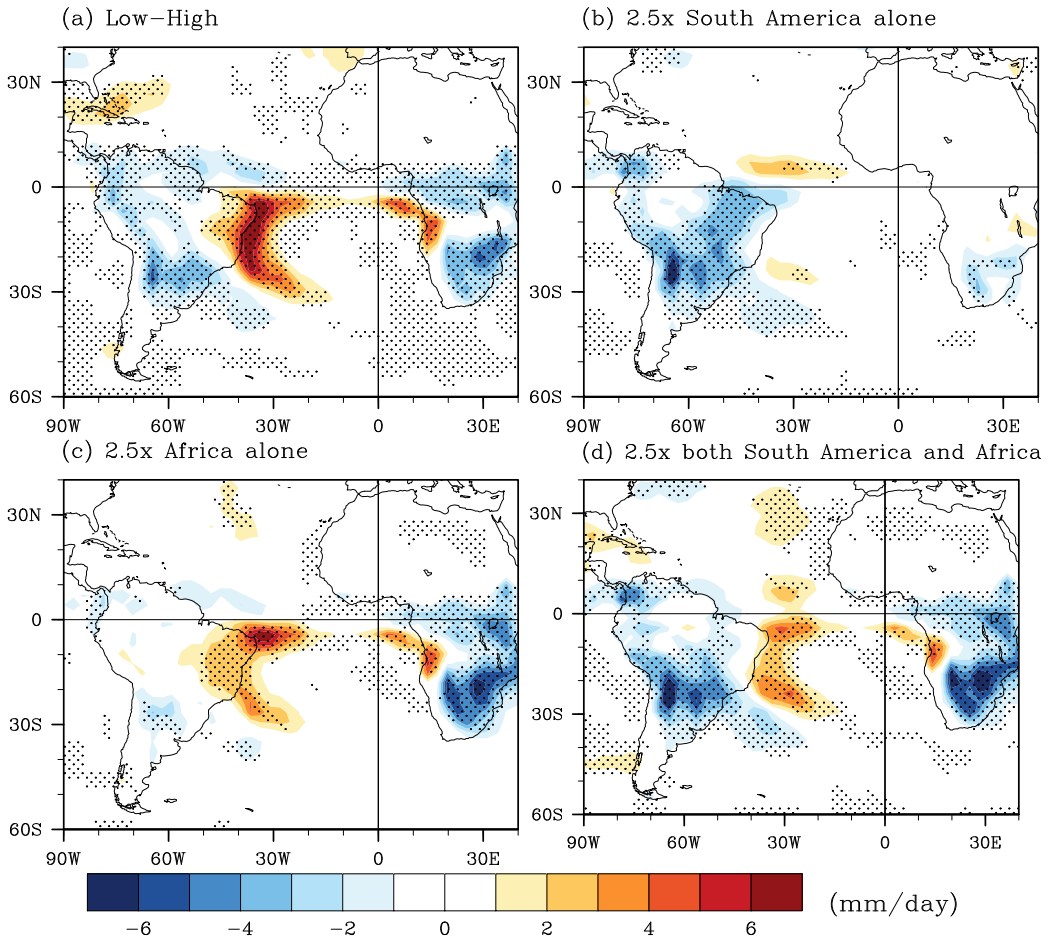

Figure 5.1: Changes in precipitation in DJF in selected experiments. (a) low insolation minus high insolation, (b) 2.5x South America alone minus highInsolation_highSST, (c) 2.5x Africa alone minus highInsolation_highSST, and (d) 2.5x both South America and Africa minus highInsolation_highSST. Stippling is as in Fig. 3.1. Shading in panel (a) is identical to shading of Fig. 3.2a.

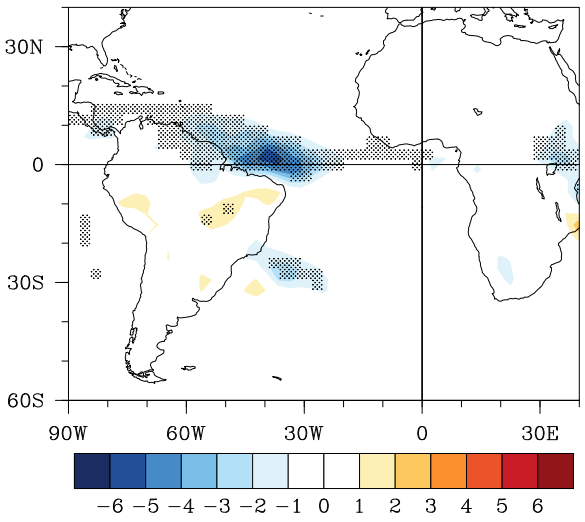

Figure 5.2: Changes in DJF precipitation: highInsolation_lowSST minus highInsolation_highSST, which hightlights the change in precipitation due to insolation-induced changes in SST. Stippling is as in Fig. 3.1.

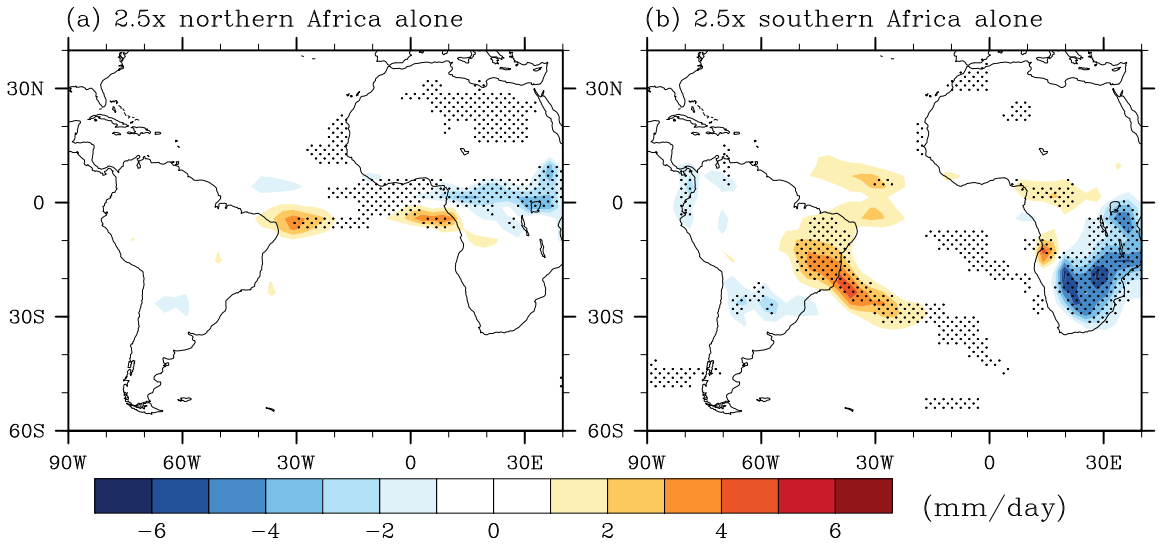

Figure 5.3: Changes in DJF precipitation in selected experiments. (a) 2.5x northern Africa alone minus highInsolation_highSST and (b) 2.5x southern Africa alone minus highInsolation_highSST. Stippling is as in Fig. 3.1.

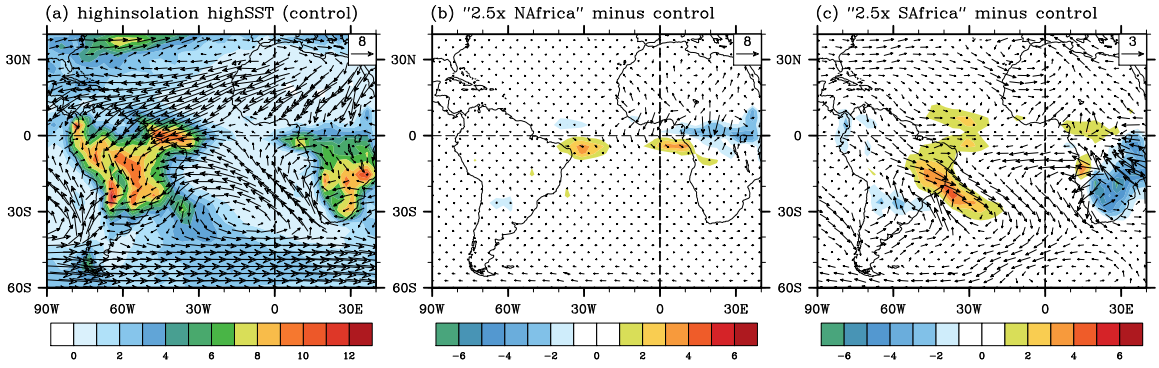

Figure 5.4: 925hPa winds (vector) and precipitation (shading) in DJF for (a) the highInsolation_highSST experiment, (b) the 2.5x northern Africa alone experiment minus highInsolation_highSST experiment, and (c) 2.5x southern Africa alone experiment minus highInsolation_highSST experiment. Scaling of the vectors is noted in the upper right corner (in m/s). Units of precipitation are mm/day.

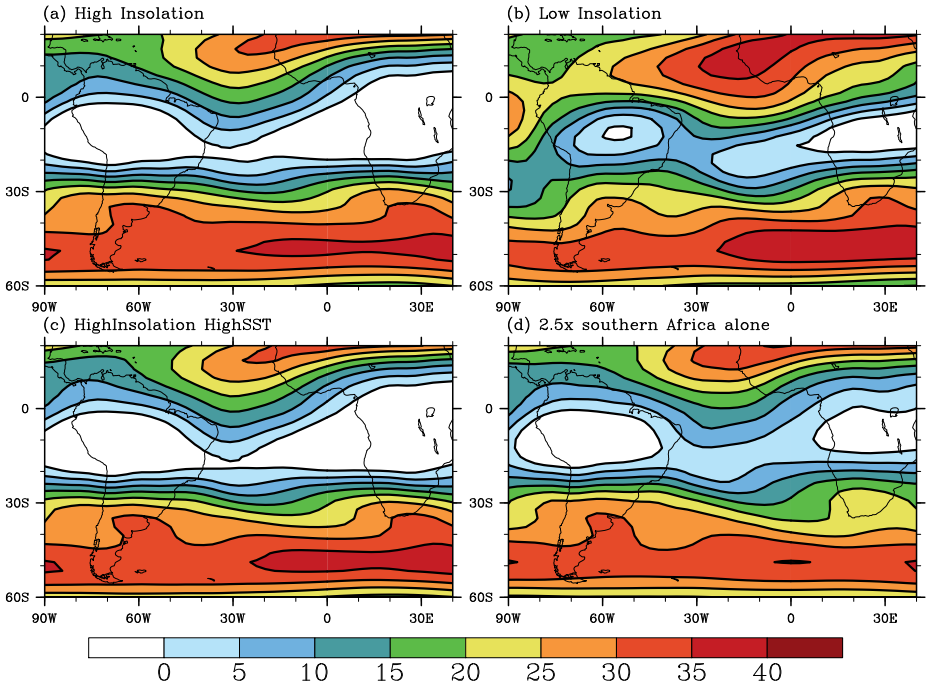

Figure 5.5: Climatological DJF zonal wind at 200hPa for: (a) high insolation, (b) low insolation, (c) highInsolation_highSST and (d) 2.5x southern Africa alone.

Chapter 6

DISCUSSION

In this chapter, we discuss how our model results compare with other proxy data and model results. We will also briefly discuss how the changes of South American monsoon differs from the changes of Asian monsoon on precessional scale.

6.1 Climatological significance of $\delta^{18}O_c$ and comparison to other proxy records

Using the decomposition method outlined in chapter 22.3, we find the causes of the orbitally forced $\delta^{18}O_p$ excursions in the Andes and eastern Brazil support the interpretation of $\delta^{18}O_c$ of speleothems offered in the literature. Specifically, our model results support the interpretation of Cruz et al. (2009) that the orbitally paced changes in $\delta^{18}O_p$ in the northeastern Brazil are due to changes in the intensity of precipitation, i.e. the "amount effect". Along the Andes, the precessional changes in $\delta^{18}O_p$ are due to changes in the $\delta^{18}O$ of the vapor arriving from the western Amazon Basin, and not solely to the"amount effect", consistent with the original interpretation by Cheng et al. (2013). Our findings about the role of water vapor are also consistent with Vuille and Werner (2005) and Vuille et al. (2012), who found that the degree of rainout of the SASM strongly impacts the isotopic composition of precipitation downstream.

The simulated orbitally forced changes in $\delta^{18}O_p$ are also consistent with the several other proxy data from the Andes that show isotopic trends over the Holocene. These include trends in $\delta^{18}O_c$ in the speleothems from Huagapo, Peru (11°S, Kanner et al. (2013)) and from Cueva del Tigre Perdido, Peru (Van Breukelen et al., 2008), trends in the $\delta^{18}O$ of authigenic calcite from Lake Junin, Peru (11°S, Seltzer et al. (2000)) and

from Laguna Pumacocha (10°S, Bird et al. (2011)) on the eastern flank of Peruvian Andes, and trends in the $\delta^{18}O$ of ice in the Huascarán glacier in the Peruvian Andes (9°S, Thompson et al. (1995)). Each of these records suggests that precipitation becomes isotopically lighter in the late Holocene (high austral summer insolation) compared to the early Holocene (low insolation). Kanner (2012) presented an older segment of the speleothem record from Huagapo Cave that extends from around 100 to 175 kbp; it also features $\delta^{18}O_c$ excursions that are clearly paced by orbital forcing, with an amplitude and phase that is consistent with the excursions simulated by the model.

The simulated changes in precipitation due to orbitally forced insolation changes also agree with other types of proxy data that are sufficiently long to resolve the precessional scale signal. These include speleothem and travertine deposits from northeastern Brazil, which feature maxima in stalagmite and travertine growth during times of high austral autumn insolation at 10°S (Wang et al., 2004), which are also times of low austral summer insolation (Fig. 2.1) and thus times whereby our models simulates high precipitation in northeastern Brazil. The natural γ-radiation record records from sediment cores in Salar de Uyuni, Bolivia (20°S) feature alternating wet and dry periods over the past 50,000 years that align well with times of high and low January insolation of 15°S, respectively (Baker et al., 2001a; Fritz et al., 2004), also in agreement with our model results. A Holocene speleothem record from Lapa Grande in the central-eastern Brazil (14°S, Stríkis et al. (2011)) is located along the southern edge of the simulated negative $\delta^{18}O_p$ in the northeastern Brazil (Fig. 3.1); as would be expected, the Lapa Grande record features a $\approx$ -0.5‰ decrease in $\delta^{18}O_p$ from 10 kbp to present. In addition to that, Haug et al. (2001) presented a record of titanium in sediments from the Cariaco Basin and argued that the ITCZ had moved southward over the course of the Holocene; this is also consistent with our results (not shown). Finally, the marine sediment core from the continental slope off the Norte Chico, Chile (27.5°S, Lamy et al. (1998)) shows dry/humid winters are associated

with high/low austral winter insolation, also consistent with our results (not shown).

There is a mismatch between the $\delta^{18}O_c$ record in the speleothems of Pacupahuain at 11°S in the Andes (11°S, Kanner et al. (2012)) and the $\delta^{18}O_p$ from our simulations; our model simulates a large (3 ‰) change in $\delta^{18}O_p$ while this speleothem record shows no orbital pacing. The likely cause for this misfit is that this record spans a limited duration when the changes in insolation are weak and when there are large changes occurring in regional precipitation that are due to changes in global ice volume (see, e.g., Stansell et al. (2014)). An analogous situation occurs in the Sanbao speleothem in eastern China: the portion of the record that spans from present to 80 kbp when insolation changes are relatively small reflects changes in global ice volume, while the portion of the record prior to 80 kbp during a time of large insolation changes overwhelmingly reflects the changes in insolation (Cheng et al., 2009).

Although there are numerous lake level reconstructions (e.g., Baker et al. (2001b); Polissar et al. (2013)) and lake $\delta^{18}O$ (e.g., Hodell et al. (1991); Curtis et al. (1999)) from the Andes over the Holocene, our high and low simulations can not be used to inform on the causes of these trends. This is because any trend in a lake level over the Holocene would be due to precipitation minus evaporation *averaged over the Holocene*. Since our high and low insolation experiments are apropos to the early and late Holocene, they can not be used to inform on the cause of a trend in lake levels. Similarly, changes in lake $\delta^{18}O$ are due to changes in the $\delta^{18}O$ of precipitation and to changes in evaporation over the course of the Holocene. Hence, the observed changes in lake $\delta^{18}O$ can only be addressed with a model of lake isotopes that is driven by the output from our climate model.

6.2 Dynamics of the precessional changes

Our model results support the hypothesis of Cruz et al. (2009) who proposed that reduced insolation in precessional cycle causes a weaker South American summer monsoon and thus less precipitation over western Amazon. They also proposed that

a weaker SASM increases the precipitation over northeatern Brazil by weakening the subsidence aloft. This is not seen in our experiments, however. Additionally, we found the DJF ITCZ moved southward in the low insolation relative to the high insolation phase, whereas Cruz et al. (2009) proposed the opposite.

Our results show that the orbitally driven changes in the heating of southern Africa influence the precipitation over and offshore of eastern South America. The mechanism appears to be a Rossby wave that is generated by the cooling of southern Africa that causes an increase in low-level time-mean (moisture) convergence in the western Tropical Atlantic, enhancing the convection in the SACZ. This is unlike the impact of Africa on the basic climatology of South America (a Walker circulation impact; see Cook et al. (2004)).

Participants in the Paleoclimate Modeling Intercomparison Project (PMIP) performed a series of experiments to examine the impact of changes in insolation between the present day and mid-Holocene (6 kbp), which are mainly due to orbitally induced changes in insolation forcing (Braconnot et al., 2002). We performed the same pair of experiments with our model; the results are shown in Fig. 6.1b. The spatial pattern of changes in DJF precipitation in our model agrees well with that from PMIP 2 (not shown) and PMIP 3 (Fig. 6.1a): precipitation decreases inland of South America and the ITCZ shifts southward in the low insolation phase (modern day) relative to the high insolation phase (Prado et al., 2013; Braconnot et al., 2007). The spatial pattern of the precipitation response of the ECHAM model to Holocene changes is also very similar to the difference between the low insolation and high insolation experiment (cf Fig. 3.2a and 6.1b), implying the response to insolation forcing is essentially linear. The only disagreement between our results and those from PMIP 3 is in South Atlantic convergence zone (SACZ), where precipitation decreases in PMIP 3 but is intensified to the north of SACZ in our model. This disagreement may be due to the inclusion of ocean dynamics in the PMIP 3 models, because changes in SACZ is seen in both our mid-Holocene experiment and 218K experiment. That ocean dynamics

is the root cause of the differences in the SACZ response is suggested by the results of Chamales (2014), who found a northward intensification and movement of SACZ in CCSM3 when CCSM3 is coupled to a slab ocean model rather than a full ocean model.

Finally, Moura and Shukla (1981), Nobre and Shukla (1996), and Mechoso et al. (1990) showed that changes in SST play an important role for interannual changes in precipitation over eastern South America, especially the droughts of northeastern Brazil. Relative to the direct changes in land heating associated with insolation forcing, however, the impact of orbitally induced changes in SST on precipitation is small. On the precessional scale, however, we show that the changes in SST have a small influence on the precipitation over South America. This finding is consistent with Liu et al. (2003) who showed that the oceanic feedback has a modest influence on South American monsoon on precessional scale, but differs from Polissar et al. (2013) who concluded that oceanic forcing plays a much larger role than previously suspected in modulating Holocene climate in South America.

6.3 Comparison to the response of the Asian Monsoon to precessional forcing

The impact of the precessional cycle on the SASM is somewhat different from that of the Indian monsoon. For the SASM, the centroid of precipitation remains over the Amazon Basin throughout the precessional cycle but waxes and wanes in intensity. In the case of the Indian monsoon, high Northern Hemisphere summer insolation features a centroid of rainfall that is over the land regions, whereas the low phase of summer insolation (such as today) features a centroid in monsoon precipitation that is over the ocean in the Bay of Bengal (Battisti et al., in review).

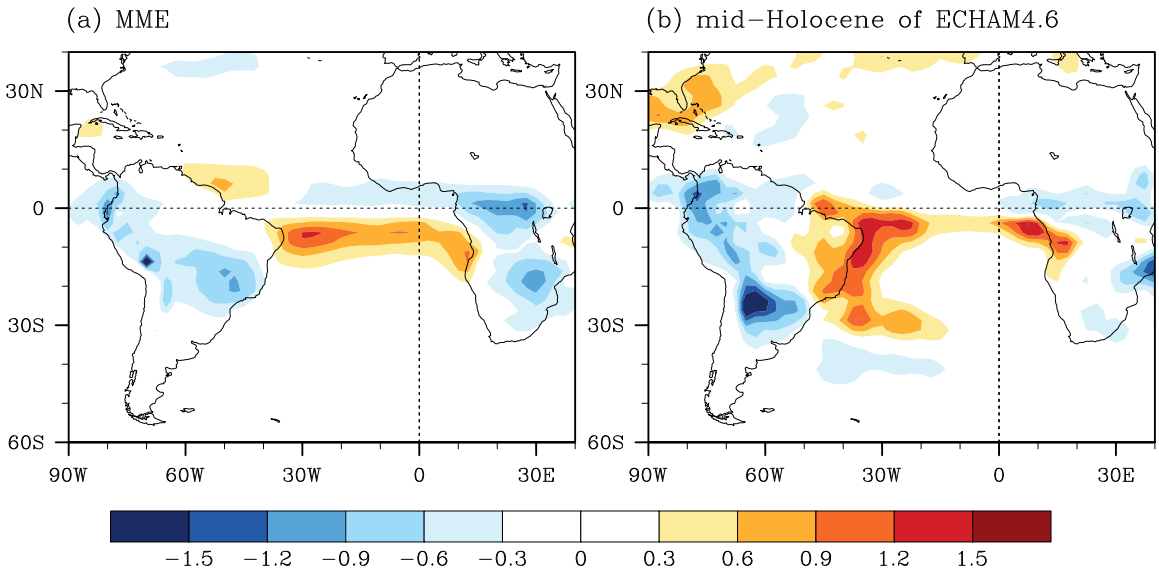

Figure 6.1: Differences in DJF precipitation between mid-Holocene and modern day climate for (a) multi-model mean of the PMIP3 models and (b) that obtained from the ECHAM4.6 model. Units of precipitation are mm/day.

Chapter 7

CONCLUSIONS

The $\delta^{18}O$ of calcite ($\delta^{18}O_c$) in speleothems of South America shows a pervasive response to orbital forcing, indicating that the tropical insolation forcing plays an important role in changing the climate of South America. We examined the climatological significance of the $\delta^{18}O_c$ using an isotope enabled general circulation model, ECHAM4.6. Two experiments were performed with the same modern-day boundary conditions, but insolation of 218,000 years ago and 207,000 years ago, defined as the "low" and "high" Southern Hemisphere summer (DJF) insolation, respectively. Differences between these two experiments display as a dipole pattern: in the low insolation experiment, precipitation increases over northeastern Brazil, but decreases over the northern Andes and the majority of inland South America; precipitation-weighted $\delta^{18}O$ ($\delta^{18}O_p$) increases in the northern Andes, but decreases in northeastern Brazil, consistent with what is seen in the $\delta^{18}O_c$ of spelothems found in these two regions.

Analysis of the changes in $\delta^{18}O_p$ reveals that the "amount effect" dominates the change in $\delta^{18}O_p$ in northeastern Brazil: compared with the high insolation phase, austral summer precipitation shifts towards more frequent heavy precipitation in the low insolation phase, which depletes the heavier isotope of precipitation and decreases the $\delta^{18}O_p$. In the northern Andes, changes in both the seasonality of precipitation and the intensity of precipitation (i.e., the "amount effect") contribute to the change in $\delta^{18}O_p$. During the low insolation phase, precipitation increases in austral winter, but decreases in austral summer, resulting in a higher ratio of winter (isotopically heavy) to summer (isotopically light) precipitation and thus higher $\delta^{18}O_p$. In addition, the vapor that condenses and precipitates on the site is heavier during the low insolation

phase, which also contributes to the increase in $\delta^{18}O_p$ in the northern Andes. The causes of the $\delta^{18}O_p$ changes in the Andes and in the northeastern Brazil are consistent with the proposed interpretation of the orbital signal in the $\delta^{18}O_c$ of stalagmites from those regions (Cruz et al., 2009; Cheng et al., 2013).

We performed three additional experiments, with surface albedo increased respectively over South America, Africa and both South America and Africa, to illuminate the processes responsible for the orbital changes in precipitation over South America. These experiments show that the decrease in summertime (DJF) precipitation inland of South America in the low insolation phase is caused by the weakening of South American summer monsoon, which is a result of the weaker local heating of land and the overlying atmosphere. The increases in precipitation in eastern South America and along the eastern coast are caused by orbital changes in the heating of Africa: weaker insolation decreases the precipitation over the southern Africa, which gives rise to a Rossby wave response to the west that enhances the low-level convergence and increases the eddy activity aloft over the South Atlantic Convergence Zone and thus increases the precipitation east and offshore of Brazil. Finally, the cooling of northern Africa in DJF shifts the Atlantic Intertropical convergence zone (ITCZ) southward, increasing the intensity of convection and decreasing the annual mean precipitation-weighted $\delta^{18}O$ ($\delta^{18}O_p$; by way of the "amount effect") over the northeastern Brazil; this is recorded in the $\delta^{18}O_c$ of speleothems. Orbitally driven changes in tropical SST contribute to the changes in precipitation in the tropical Atlantic north of Brazil; elsewhere changes in SST have a negligible impact on climate and the isotopic composition of precipitation.

BIBLIOGRAPHY

Baker, P. A., C. A. Rigsby, G. O. Seltzer, S. C. Fritz, T. K. Lowenstein, N. P. Bacher, and C. Veliz, 2001a: Tropical climate changes at millennial and orbital timescales on the Bolivian Altiplano. *Nature*, **409 (6821)**, 698–701.

Baker, P. A., et al., 2001b: The history of South American tropical precipitation for the past 25,000 years. *Science*, **291 (5504)**, 640–643.

Battisti, D. S., Q. Ding, and G. H. Roe, 2014: Coherent pan-Asian climate and isotopic response to precessional forcing. *Journal of Geophysical Research: Atmospheres*, **Submitted**.

Bird, B. W., M. B. Abbott, D. T. Rodbell, and M. Vuille, 2011: Holocene tropical South American hydroclimate revealed from a decadally resolved lake sediment $\delta^{18}O$ record. *Earth and Planetary Science Letters*, **310 (3)**, 192–202.

Braconnot, P., M. Loutre, B. Dong, S. Joussaume, and P. Valdes, 2002: How the simulated change in monsoon at 6 ka BP is related to the simulation of the modern climate: results from the Paleoclimate Modeling Intercomparison Project. *Climate Dynamics*, **19 (2)**, 107–121.

Braconnot, P., et al., 2007: Results of PMIP2 coupled simulations of the Mid-Holocene and Last Glacial Maximum–Part 1: experiments and large-scale features. *Climate of the Past*, **3 (2)**, 261–277.

Chamales, K. A., 2014: The effects of orbital precession on tropical precipitation. M.S. thesis, University of Miami.

Cheng, H., R. L. Edwards, W. S. Broecker, G. H. Denton, X. Kong, Y. Wang, R. Zhang, and X. Wang, 2009: Ice age terminations. *science*, **326 (5950)**, 248–252.

Cheng, H., et al., 2013: Climate change patterns in Amazonia and biodiversity. *Nature Communications*, **4**, 1411.

Cook, K., J. Hsieh, and S. Hagos, 2004: The Africa-South America intercontinental teleconnection. *Journal of Climate*, **17 (14)**, 2851–2865.

Cruz, F. W., et al., 2005: Insolation-driven changes in atmospheric circulation over the past 116,000 years in subtropical Brazil. *Nature*, **434 (7029)**, 63–66.

Cruz, F. W., et al., 2009: Orbitally driven east–west antiphasing of South American precipitation. *Nature Geoscience*, **2 (3)**, 210–214.

Curtis, J. H., M. Brenner, and D. A. Hodell, 1999: Climate change in the Lake Valencia Basin, Venezuela, $\sim$ 12600 yr BP to present. *The Holocene*, **9 (5)**, 609–619.

deMenocal, P. and J. Tierney, 2012: Green Sahara: African humid periods paced by Earth's orbital changes. *Nat Educ Knowl*, **3 (10)**, 12.

Dettinger, M. D., D. S. Battisti, R. Garreaud, G. McCabe, and C. Bitz, 2001: Interhemispheric effects of interannual and decadal ENSO-like climate variations on the Americas. *Interhemispheric Climate Linkages*, 1–16.

Donohoe, A. and D. S. Battisti, 2011: Atmospheric and surface contributions to planetary albedo. *Journal of Climate*, **24 (16)**, 4402–4418.

Fritz, S. C., et al., 2004: Hydrologic variation during the last 170,000 years in the southern hemisphere tropics of South America. *Quaternary Research*, **61 (1)**, 95–104.

Garreaud, R. D., M. Vuille, R. Compagnucci, and J. Marengo, 2009: Present-day South American climate. *Palaeogeography, Palaeoclimatology, Palaeoecology*, **281 (3)**, 180–195.

Gill, A., 1980: Some simple solutions for heat-induced tropical circulation. *Quarterly Journal of the Royal Meteorological Society*, **106 (449)**, 447–462.

Haug, G. H., K. A. Hughen, D. M. Sigman, L. C. Peterson, and U. Röhl, 2001: Southward migration of the intertropical convergence zone through the Holocene. *Science*, **293 (5533)**, 1304–1308.

Hodell, D. A., J. H. Curtis, G. A. Jones, A. Higuera-Gundy, M. Brenner, M. W. Binford, and K. T. Dorsey, 1991: Reconstruction of Caribbean climate change over the past 10, 500 years. *Nature*, **352 (6338)**, 790–793.

Hoffmann, G., M. Werner, and M. Heimann, 1998: Water isotope module of the ECHAM atmospheric general circulation model: A study on timescales from days to several years. *Journal of Geophysical Research*, **103 (D14)**, 16 871–16.

Kanner, L. C., 2012: An isotopic perspective on climatic change in tropical South America from the modern through the Last Glacial period. Ph.D. thesis, University of Massachusetts - Amherst.

Kanner, L. C., S. J. Burns, H. Cheng, and R. L. Edwards, 2012: High-latitude forcing of the South American summer monsoon during the last glacial. *Science*, **335 (6068)**, 570–573.

Kanner, L. C., S. J. Burns, H. Cheng, R. L. Edwards, and M. Vuille, 2013: High-resolution variability of the South American summer monsoon over the last seven millennia: insights from a speleothem record from the central Peruvian Andes. *Quaternary Science Reviews*, **75**, 1–10.

Kodama, Y.-M., 1993: Large-scale common features of subtropical convergence zones (the Baiu frontal zone, the SPCZ and the SACZ) Part II: Conditions of the circulations for generating the STCZs. *J. Meteor. Soc. Japan*, **71**, 581–610.

Kutzbach, J. E. and P. J. Guetter, 1986: The influence of changing orbital parameters and surface boundary conditions on climate simulations for the past 18 000 years. *Journal of the Atmospheric Sciences*, **43 (16)**, 1726–1759.

Lamy, F., D. Hebbeln, and G. Wefer, 1998: Late Quaternary precessional cycles of terrigenous sediment input off the Norte Chico, Chile (27.5 S) and palaeoclimatic implications. *Palaeogeography, Palaeoclimatology, Palaeoecology*, **141 (3)**, 233–251.

Lee, J.-E. and I. Fung, 2008: "Amount effect" of water isotopes and quantitative analysis of post-condensation processes. *Hydrological Processes*, **22 (1)**, 1–8.

Liu, Z., B. Otto-Bliesner, J. Kutzbach, L. Li, and C. Shields, 2003: Coupled Climate Simulation of the Evolution of Global Monsoons in the Holocene. *Journal of Climate*, **16 (15)**, 2472–2490.

Mechoso, C. R., S. W. Lyons, and J. A. Spahr, 1990: The impact of sea surface temperature anomalies on the rainfall over northeast Brazil. *Journal of Climate*, **3 (8)**, 812–826.

Mosblech, N. A., et al., 2012: North Atlantic forcing of Amazonian precipitation during the last ice age. *Nature Geoscience*, **5 (11)**, 817–820.

Moura, A. D. and J. Shukla, 1981: On the dynamics of droughts in northeast Brazil: Observations, theory and numerical experiments with a general circulation model. *Journal of the Atmospheric Sciences*, **38 (12)**, 2653–2675.

Nobre, P. and J. Shukla, 1996: Variations of sea surface temperature, wind stress, and rainfall over the tropical Atlantic and South America. *Journal of Climate*, **9 (10)**, 2464–2479.

Philander, S., D. Gu, G. Lambert, T. Li, D. Halpern, N. Lau, and R. Pacanowski, 1996: Why the ITCZ is mostly north of the equator. *Journal of Climate*, **9 (12)**, 2958–2972.

Polissar, P. J., M. B. Abbott, A. P. Wolfe, M. Vuille, and M. Bezada, 2013: Synchronous interhemispheric holocene climate trends in the tropical andes. *Proceedings of the National Academy of Sciences*, **110 (36)**, 14 551–14 556.

Prado, L. F., I. Wainer, and C. M. Chiessi, 2013: Mid-Holocene PMIP3/CMIP5 model results: Intercomparison for the South American monsoon system. *The Holocene*, **23 (12)**, 1915–1920.

Roeckner, E., 1996: Coauthors, 1996: The atmospheric general circulation model ECHAM-4: Model description and simulation of present-day climate. *Max-Planck-Institut für Meteorologie Rep*, **218**, 90.

Seltzer, G., D. Rodbell, and S. Burns, 2000: Isotopic evidence for late Quaternary climatic change in tropical South America. *Geology*, **28 (1)**, 35–38.

Stansell, N. D., P. J. Polissar, M. B. Abbott, M. Bezada, B. A. Steinman, and C. Braun, 2014: Proglacial lake sediment records reveal Holocene climate changes in the Venezuelan Andes. *Quaternary Science Reviews*, **89**, 44–55.

Stríkis, N. M., et al., 2011: Abrupt variations in South American monsoon rainfall during the Holocene based on a speleothem record from central-eastern Brazil. *Geology*, **39 (11)**, 1075–1078.

Thompson, L. G., E. Mosley-Thompson, M. E. Davis, P.-N. Lin, K. A. Henderson, J. Cole-Dai, J. F. Bolzan, and K.-B. Liu, 1995: Late glacial stage and Holocene tropical ice core records from Huascaran, Peru. *Science*, **269 (5220)**, 46–50.

Van Breukelen, M., H. Vonhof, J. Hellstrom, W. Wester, and D. Kroon, 2008: Fossil dripwater in stalagmites reveals Holocene temperature and rainfall variation in Amazonia. *Earth and Planetary Science Letters*, **275 (1)**, 54–60.

Vera, C., et al., 2006: Toward a unified view of the American monsoon systems. *Journal of Climate*, **19 (20)**, 4977–5000.

Vuille, M. and M. Werner, 2005: Stable isotopes in precipitation recording south american summer monsoon and enso variability: observations and model results. *Climate Dynamics*, **25 (4)**, 401–413.

Vuille, M., et al., 2012: A review of the south american monsoon history as recorded in stable isotopic proxies over the past two millennia. *Climate of the Past*, **8 (4)**, 1309–1321.

Waliser, D. E. and C. Gautier, 1993: A satellite-derived climatology of the ITCZ. *Journal of Climate*, **6 (11)**, 2162–2174.

Wang, X., A. S. Auler, R. Edwards, H. Cheng, E. Ito, Y. Wang, X. Kong, and M. Solheid, 2007: Millennial-scale precipitation changes in southern Brazil over the past 90,000 years. *Geophysical Research Letters*, **34 (23)**, L23 701.

Wang, X., A. S. Auler, R. L. Edwards, H. Cheng, P. S. Cristalli, P. L. Smart, D. A. Richards, and C.-C. Shen, 2004: Wet periods in northeastern Brazil over the past 210 kyr linked to distant climate anomalies. *Nature*, **432 (7018)**, 740–743.

Xie, P. and P. A. Arkin, 1997: Global precipitation: A 17-year monthly analysis based on gauge observations, satellite estimates, and numerical model outputs. *Bulletin of the American Meteorological Society*, **78 (11)**, 2539–2558.

Yulaeva, E. and J. M. Wallace, 1994: The signature of ENSO in global temperature and precipitation fields derived from the microwave sounding unit. *Journal of Climate*, **7 (11)**, 1719–1736.

Zhou, J. and K. Lau, 1998: Does a monsoon climate exist over South America? *Journal of Climate*, **11 (5)**, 1020–1040.

Appendix A

DERIVATION OF THE SCALING FACTOR USED IN THE "INCREASING ALBEO" EXPERIMENTS

The "increasing albedo" experiments in Section 5 are designed to illuminate the changes in precipitation and circulation that are due to local, regional scale changes in the precessional forcing. Since the climate model does not allow localized changes in the downward top-of-the-atmosphere radiation, we approximated the regional changes in the insolation forcing associated with the low insolation forcing by altering the surface albedo. The factor of 2.5 used in these "increasing albedo" experiments is derived as follows.

Following the the method of Donohoe and Battisti (2011), we decompose the planetary albedo α_p into the surface contribution α_{surf} and atmospheric contribution α_{atmos}

$$\alpha_p \quad = \alpha_{atmos} \quad + \quad \alpha_{surf} \quad , \tag{A.1}$$

where the surface contribution α_{surf} is:

$$\alpha_{surf} \quad = \alpha \frac{(1 - R - A)^2}{1 - \alpha R} \quad . \tag{A.2}$$

In Eq. A2, A is the fraction of insolation that is absorbed within the atmosphere; R is the fraction of the insoaltion that is reflected by the atmosphere (atmospheric contribution to the planetary albedo), and α is the surface albedo. A change in the surface contribution to planetary albedo $\Delta\alpha_{surf}$ induced by a change in the surface

albedo $\Delta\alpha$ can then be written as:

$$\Delta\alpha_{surf} = (\alpha + \Delta\alpha)\frac{(1-R-A)^2}{1-(\alpha+\Delta\alpha)R} - \alpha\frac{(1-R-A)^2}{1-\alpha R} \quad . \tag{A.3}$$

Values of A, R, α and α_{surf} are taken from the high insolation (207 kbp) experiment. Holding A, R and α_{atmos} constant, $\Delta\alpha_{surf}$ is:

$$\Delta\alpha_{surf} = \frac{\Delta SW_{net}}{S_0} \quad , \tag{A.4}$$

where S_0 is the incoming solar radiation at the top of the atmosphere, and ΔSW_{net} is the net downward shortwave radiation at the top of the atmosphere that is seen in the response to precessional forcing:

$$\Delta SW_{net} = SW_{net}(218kbp) - SW_{net}(207kbp) \quad . \tag{A.5}$$

Plugging in the DJF values of A, R, α and S_0 from the high insolation (207 kbp) experiment, as well as the orbitally induced change in DJF insolation ΔSW_{net}, we estimate the increase in surface albedo to be a factor of 2.5. Figure A1 shows that the increase in surface albedo by a factor of 2.5 gives the similar net TOA radiation change that is seen in the low insolation minus high insolation experiments (cf panels e and f in Fig. A1).

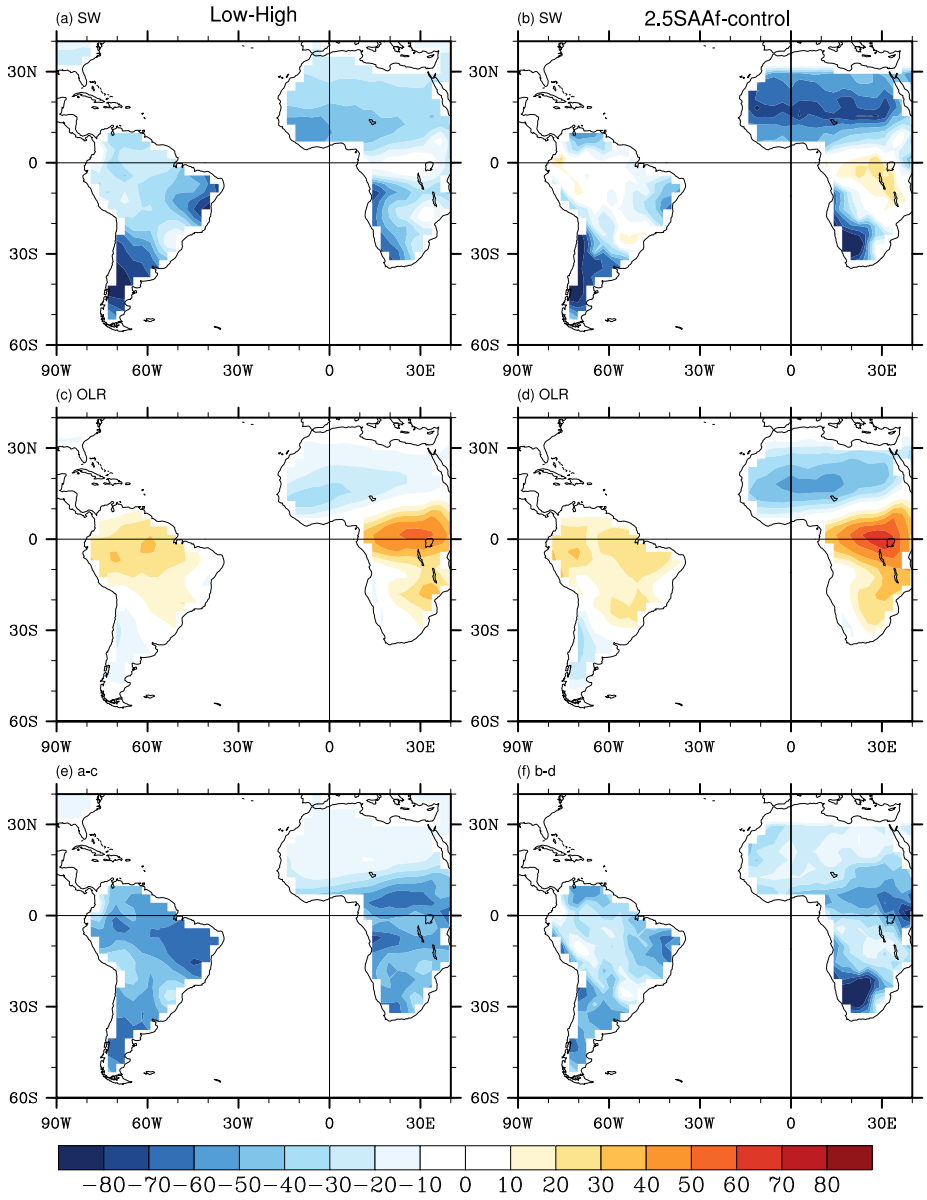

Figure A.1: Differences in (a) net shortwave radiation (SW) at top of the atmosphere (TOA), (c) outgoing longwave radiation (OLR) and (e) net radiation at TOA, that is OLR minus net SW at TOA for the low insolation minus high insolation experiment. b, d and f are the same as a, c and e, but for 2.5x both South America and Africa minus highInsolation_highSST experiment.